The role of the pulsed laser deposition in different growth atmospheres on the gas-sensing properties of ZnO films

Kamran Syed[1, *], Nikša Krstulović[2], Juan Casanova-Cháfer[3], Eduard Llobet[3], Frank Güell[3,4], Paulina R. Martínez-Alanis[4], Marijan Marciuš[1], Ekaterina Shagieva[5], Davor Ristić[1], Hrvoje Gebavi[1], Nikola Baran[1], Mile Ivanda[1, *]

[1]*Ruđer Bošković Institute, Bijenička cesta 54, 10000, Zagreb, Croatia*
[2]*Institute of Physics, Bijenička cesta 46, 10000 Zagreb, Croatia*
[3]*MINOS, Universitat Rovira i Virgili, Avda. Països Catalans, 26, 43007, Tarragona, Spain*
[4]*ENFOCAT-IN[2]UB, Universitat de Barcelona, C/Martí i Franquès 1, 08028 Barcelona, Catalunya, Spain*
[5]*Institute of Physics of the Czech Academy of Sciences, Cukrovarnick´a 10, 16200 Prague, Czech Republic*

* Corresponding authors email: kamran.syed.siegen@gmail.com, ksyed@irb.hr, ivanda@irb.hr

Abstract

ZnO films were fabricated by pulsed laser deposition using two different background atmospheres (argon/vacuum). The gas-sensing properties of these materials against reducing and oxidizing gases were examined. The microstructure and crystal symmetry of the deposited films were studied with X-ray diffraction (XRD), Scanning electron microscopy (SEM), X-ray photoelectron spectroscopy (XPS), Raman, and Photoluminescence (PL) spectroscopy. The XRD studies revealed that the ZnO films grown in an argon environment are highly textured in the c-axis with a hexagonal crystalline structure. The c-axis is perpendicular to the substrate plane orientation (002) compared to (100) plane orientation, which is developed in a vacuum environment. Usually, this orientation (100) is difficult to obtain. Raman scattering spectra for both types of ZnO films revealed the characteristic E_2 (high) mode that is related to the vibration of oxygen atoms in wurtzite ZnO. Moreover, PL spectra showed that a high number of defects appear in both the vacuum and argon-grown ZnO films. XPS data indicated that the O1*s* peak consists of several components identified as lattice oxygen, oxygen close to defects, and chemisorbed species. Furthermore, gas-sensing properties were investigated for nitrogen dioxide (NO_2) at different

operating temperatures and concentrations. Although both types of ZnO films have shown a good response towards NO_2 at ppb levels, the films prepared under vacuum conditions showed higher responses. This was attributed to differences in crystallinity, microstructure, and the type of defects present in these materials.

Keywords: ZnO, PLD technique, different atmospheres, gas sensors, photoluminescence, surface defects, enhanced recovery, NO_2

1. Introduction

The World Health Organization (WHO) has warned that air pollution levels are often above the maximum safe levels (threshold limit values TLV) for key pollutants as such nitrogen dioxide (NO_2) [1]. It leads to climate change and its exposure can cause a variety of adverse health outcomes for humans, animals, and plants. The immense increase in air pollution is associated with seven million deaths yearly [2]. NO_2 exposure is linked to conditions such as heart disease and strokes [3]. It can reduce lung growth in children, cause aggravated asthma, and damage buildings [4]. Several steps are being taken to help reduce air pollution levels across the globe. Governments are enforcing stringent pollution norms to move from coal and gas power stations and diesel generators to solar, wind, and hydropower and shift to electric cars technology [5]. Prioritizing walking, cycling, and public transport over cars in urban areas, and deterring polluting vehicles from city and town centers is the quickest, most cost-effective way to cut nitrogen dioxide pollution levels, which are illegal in most urban areas [6]. The taking over of fossil fuel energy sources for renewable ones is progressive, however real-time detection and monitoring of the concentration of harmful and poisonous pollutants are required [7].

Gas mixture instrumental analysis such as (GC-MS), ion mobility spectrometry (IMS), and proton-transfer-reaction mass spectrometry (PTR-MS) show significant drawbacks [8]. These techniques require high operational costs, complicated miniaturization, and time-consuming sample preparation and analysis. Other approaches, like electrochemical sensors, have confined temperature ranges and shorter life spans [9]. This has motivated significant efforts for the development of sensors in the area of research to improve the levels of gas detection [10]. For that reason, chemoresistive sensors have emerged as a promising candidate, as they offer a more rapid,

user-friendly, miniaturized, non-destructive, and affordable detection of several toxic gases both with high sensitivity and fair selectivity [11].

Chemoresistive sensors based on metal oxide (MOX) have been studied in the research area of environmental monitoring, automotive, biomedical, food quality control, etc. [12]. These devices usually show simple measuring electronics, high sensitivity to gases, fast response, recovery dynamics, and sensor-to-sensor reproducibility [13],[14].

Among metal oxides, ZnO is a broad band gap (near 3.4 eV) semiconductor at room temperature [14]. Also, ZnO II−VI is an n-type semiconductor with high exciton binding energy (~60 meV), non-toxicity, high surface-to-volume ratio, low cost, suitability to doping, and considerable sensitivity [15],[16],[17]. Due to these distinctive properties, it has been considered one of the most favorable materials for gas sensing, solar cells [18],[19], lasers [20], thin film transistors [21], light emitting diode [22], nanophotonic and piezoelectric devices [23],[24]. Different nanostructures of ZnO including nanorods [25], nanowires [26], and nanoflowers [27], can be deposited on various substrates using a variety of methodologies, such as magnetron sputtering [28], thermal evaporation [29], and atomic layer deposition [30].

A recent report indicated that the use of gas sensing properties of pulsed laser deposition (PLD) of ZnO films is strongly dependent on the nature of the crystal surface exposed to the gas species for H_2 [31],[32]. The reports on EtOH and CO_2 sensing properties of ZnO fabricated by PLD in the air atmospheric pressure revealed the highest response attributed to adsorbed oxygen species [33]. Also, the photoluminescence (PL) of the PLD ZnO films annealed in the vacuum has shown differences in spectral features compared to argon atmosphere annealed films. It has been proposed that the broad luminescence is due to a zinc vacancy acceptor, a complex defect involving zinc interstitials, zinc–oxygen, anti-site defects, and oxygen vacancies [34]. Additionally, The detection of NO_2 and NH_3 at 10 ppm deposited onto polycor substrates under oxygen conditions was reported [35]. The sensing properties were attributed to the dependence of the grain size on the target substrate distance [35]. Despite the effort made in recent years to apply different background atmospheres to PLD ZnO films, most works have been focused on improving gas sensing, limited to applying changes in the oxygen pressure or in the mixture of oxygen and argon background conditions for the growth of PLD ZnO films [36],[37],[38],[39]. In addition, the available knowledge is still limited for ZnO films (i.e., their microstructure, optical properties and, gas

sensing properties) grown via PLD under argon-vacuum background conditions [40],[41],[42],[43],[44].

To the best of our knowledge, the role of argon and vacuum background atmosphere on the gas sensing properties of ZnO films grown via a self-catalyzed PLD process (i.e., without using metal catalyst) has not been reported yet. In this regard, we propose for the first time, the successful synthesis of ZnO films via a self-catalyzed PLD method using two different background atmospheres (argon/vacuum) for the fabrication of NO_2 gas sensors. The structure, crystallinity, optical properties, and chemical composition of the ZnO films are characterized by FESEM, XRD, Raman, PL and, X-ray photoelectron spectroscopy (XPS). Moreover, the gas sensing properties towards the detection of NO_2 of vacuum and argon-grown ZnO films are investigated and compared. The link between point defects, gas sensing behavior, XPS and, PL results are discussed.

2. Experimental Section

2.1. Synthesis of ZnO films

The PLD films were obtained by laser ablation of a solid ZnO target onto silicon and alumina substrates, using the wavelength (1064 nm) of an Nd: YAG laser operating at 5 Hz with a pulse duration of 5 ns, and output energy of 340 mJ. The laser pulse energy in front of the target was 150 mJ. The Schematic view of the pulsed laser deposition setup is presented in Fig.1. At a laser power density of 40 J/cm^2, ZnO films were obtained after 5000 shots onto p-type Si (100) substrates, either under an Argon operating pressure of 30Pa (0.3mbar) (>99.99% purity) or under a vacuum pressure < 10^{-3} mbar. The distance between the target and substrate was 3 cm. The ZnO target surface was kept parallel to the substrate and inclined by 45 degrees concerning the impinging laser pulses. Both the target holder and the substrate were kept on floating potential, at room temperature and were rotated during deposition to avoid the drilling of the target and to increase the homogeneity of the deposited films. After deposition, annealing was done for both types of films under vacuum at 500 ◦C for 2h in a quartz furnace tube to obtain crystallinity. Sample thickness was estimated via focused ion beam (FIB) assisted cross-sectional SEM. Vacuum grown samples and argon grown samples were typically 190 ± 20 nm and 90 ± 14 nm thick, respectively.

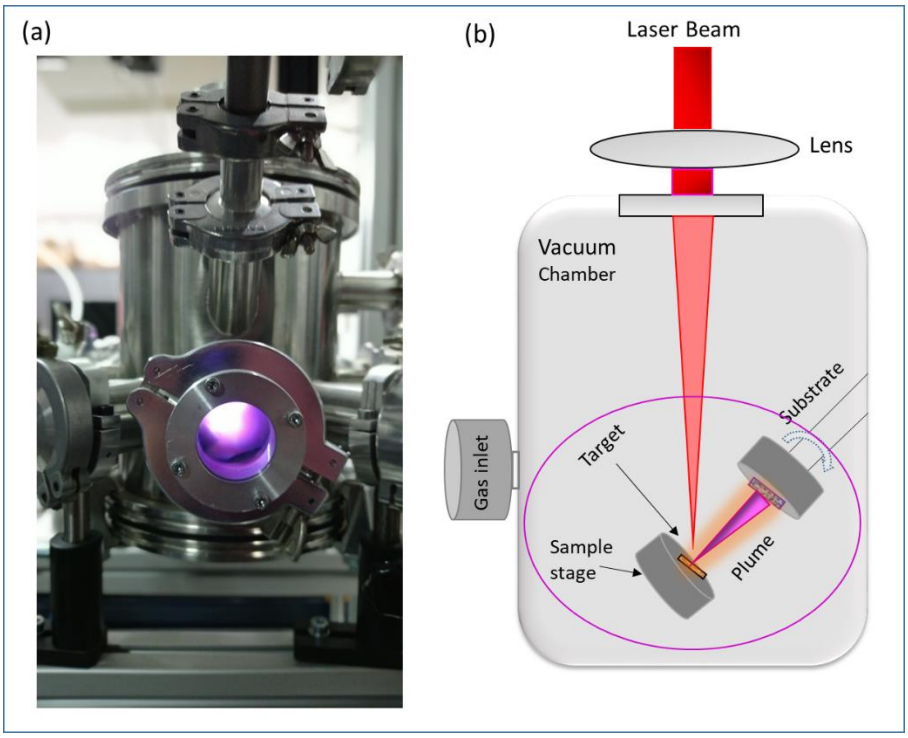

Fig. 1 (a) Actual PLD setup used in this work (b) Schematic view of pulsed laser deposition setup.

2.2. Characterization of the gas-sensitive materials

The crystalline structure of the ZnO films was studied by XRD using the Siemens D5000 diffractometer equipped with Cu anode, Goebel mirror, and graphite monochromator in front of the point detector. The experiments were performed in the grazing incidence geometry using λ = 1.5406 Å ranging from 20º to 80º (2θ) with a scanning step size of 0.020°. A Field Emission Scanning Electron Microscope (JSM-7500F) was used to examine the surface morphology of the samples. XPS measurements have been performed in a PHI 5500 Multitechnique System equipped with a monochromatic X-ray radiation source of Al Kα (1486.6 eV) at 350 W. The sample was placed perpendicular to the analyzer axis and calibrated using the $3d_{5/2}$ line of Ag with a full width at half maximum (FWHM) of 0.8 eV. The diameter circle of the analyzed area was 0.8 mm. The resolution for the general and depth profile spectra was 187.5 eV of pass energy at 0.8 eV/step, and 23.5 eV of pass energy at 0.1 eV/step, respectively. All measurements were made in an ultra-

high vacuum (UHV) chamber pressure ($5 \cdot 10^{-9}$ and $2 \cdot 10^{-8}$ torr). The binding energies (BE) values were referred to as the C 1s BE at 284.8 eV. Component analysis has been performed by constructive curve joint Shirley and Tougaard functions to determine the peak background, and the line shape of the curves was fitted with mixed Lorentzian-Gaussian at 10-30% ratio. Optical characterization was carried out by the Raman spectroscopy by a Renishaw In Via Reflex Raman spectrometer with a 325 nm excitation, and room-temperature PL measurements were made using a chopped Kimmon IK Series He-Cd laser (325 nm and 40 mW). Fluorescence was dispersed with an Oriel Corner Stone 1/8 74000 monochromator, detected using a Hamamatsu H8259-02 with a socket assembly E717-500 photomultiplier, and amplified through a Stanford Research Systems SR830 DSP. A filter in 360 nm was used to stray light. All spectra were corrected for the response function of the setups.

2.3. Device fabrication and gas-sensing measurements

In this paper, alumina substrates (with 3-micron thick, platinum screen-printed electrodes) were coated with ZnO films by the PLD technique to achieve chemoresistive gas sensors. Commercially available substrates from CeramTech GmbH were used. The electrode area is 5×2.5 mm^2 and the width of interdigitated electrode fingers and electrode gap are 300 microns. The response towards nitrogen dioxide at 200, 400, 600, 800, and 1000 ppb was studied. The gas sensing measurements were performed inside the 35 cm^3 airtight Teflon chamber. The change in the electrical resistance of ZnO films was monitored by a multimeter (HP 34972A, Agilent) data acquisition system. The sensors were kept under dry air for 30 min before being exposed in repeated cycles to a given concentration of nitrogen dioxide species for 5 min. The total flow rate of gas was adjusted to 100 mL/min using a (Bronkhorst High-Tech B.V.) mass-flow gas control system that delivers reproducible concentrations of the gas tested. Gas sensing measurements were carried out in repeated cycles that consist of 30 min of exposure to a given gas concentration, followed by 30 min under dry air for cleaning and baseline recovery.

3. Results and discussion

3.1. Structural and morphological studies

The crystal structures and phase of the PLD-grown ZnO films in vacuum and argon atmosphere were analyzed by XRD, as shown in Fig 2

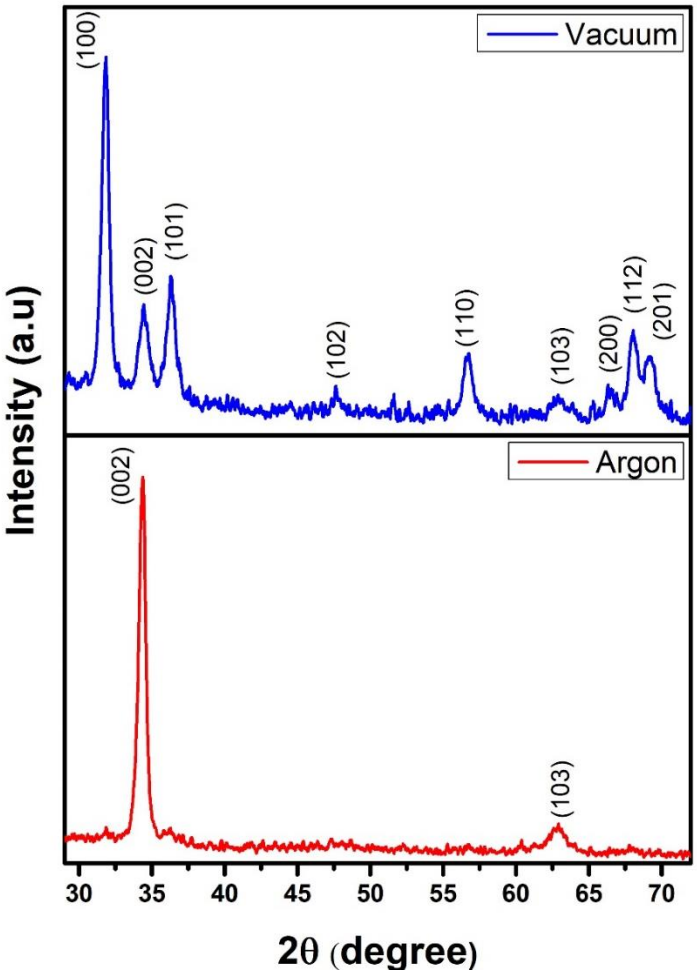

Fig. 2. XRD diffractograms of ZnO films fabricated by Pulse laser deposition on silicon substrate using two different background atmospheres (Argon/Vacuum).

The diffraction patterns for both types of films are indexed to the hexagonal wurtzite phase of ZnO in accordance with JCPDS card no. 00-36-1451. The strong and sharp peaks show the good crystallinity of the synthesized materials. Further, the average crystallite sizes of prepared samples were calculated using Scherer's formula from the XRD patterns and found to be about 51 nm and 29 nm for vacuum and argon-grown ZnO films, respectively. The ZnO films grown by PLD in an argon environment are highly oriented in the c-axis of the hexagonal ZnO wurtzite structure. The intense (002) peak dominates the diffraction pattern, in addition a low intensity ZnO diffraction (103) peak was observed. We note that the intensity is some three orders of magnitude lower than the peak for the (002) reflection. A dominant diffraction peak for the (002) plane at $2\theta = 34.35^{\circ}$ indicates a high degree of anisotropic growth of ZnO nanograins. The peak is very strong and narrow, demonstrating a high degree of crystallinity of the fabricated ZnO film. This is in line with the characteristics of the hexagonal ZnO wurtzite where the *c*-axis is perpendicular to the substrate plane [45],[46].

In contrast, the diffractogram associated to ZnO grown under vacuum conditions, a significantly higher number of reflecting planes are visible. Nine diffraction peaks were observed at 31.82˚, 34.48˚, 36.38˚, 47.66˚, 56.68˚, 62.89˚, 66.43˚, 68.08˚ and 69.36˚ corresponding to the (100), (002), (101), (102), (110), (103), (200), (112) and (201) planes of hexagonal ZnO, indicating formation of polycrystalline films under vacuum. No other impurity peaks were observed in the XRD pattern.

Surface morphology studies of ZnO films have been conducted using FESEM. Fig. 3 shows the FESEM images of ZnO films at a high resolution. ZnO films grown under a vacuum atmosphere present clusters composed of multiple grains with sharp edges, suggesting a polycrystalline growth with different crystallites showing up on the surface. In ZnO films grown under argon the clusters tend to merge, forming a more compact and uniform structure composed of small grains with well-rounded shapes. The grain size of ZnO films is higher when grown in a vacuum atmosphere than when grown under an argon atmosphere.

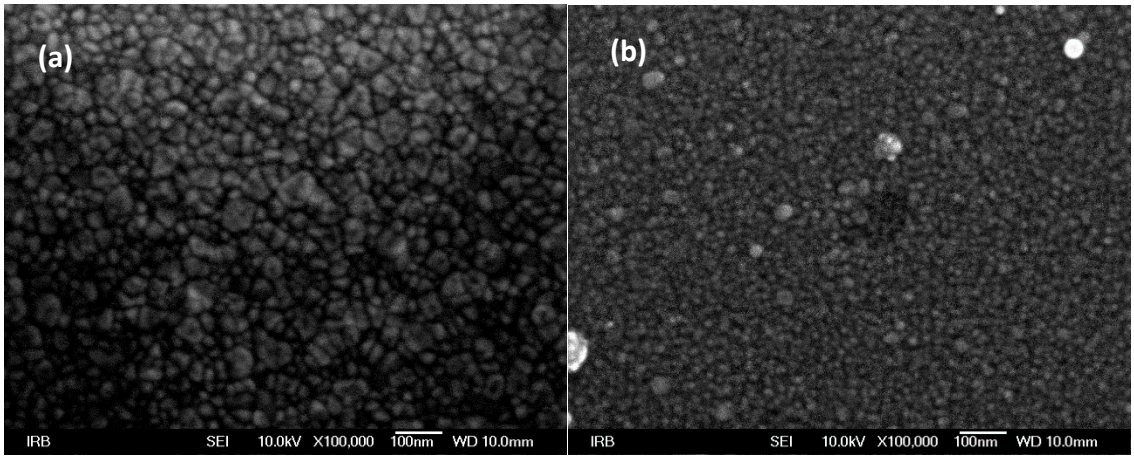

Fig. 3. The SEM morphology after annealing of ZnO films deposited in different growth atmospheres (a) vacuum and (b) argon.

3.2. Chemical analysis by XPS

Fig. 4. shows the results obtained by XPS analysis. The full spectra in Fig. 4(a) shows the main peaks according to the expected atoms. The XPS analysis was performed using internal charge reference to C 1s at 284.8 eV. Besides the C 1s peak corresponding to adventitious carbon, a low-intensity peak at 287-290 eV region was assigned to the presence of carbonate species [47]; these carbonate species could be formed from CO_2 when the samples are exposed to ambient conditions. Interestingly, just a low-intensity signal of Si is observed on both samples, which reflects a complete surface coating with the ZnO films over the Si substrates. Fig. 4(b) shows the spectra corresponding to the Zn 2*p*3 core level, and its deconvolution in two components at around 1021.9 and 1023.8 eV corresponding to the lattice zinc (Zn-O) in the wurtzite structure and zinc interstitials (Zn_i) or chemisorbed species, respectively. Fig. 4 (c) shows the spectra corresponding to the O 1*s* core level, which can be deconvoluted into four components. The bands centered at around 530.2 and 531.3 eV binding energies are related to lattice oxygen (O-Zn) in the wurtzite structure and oxygen vacancies (V_O), respectively. The broad band centered at around 532.0 eV binding energy indicates the presence of hydroxyl groups (OH), and the band centered at around 533.3 eV is related to oxygen interstitials (O_i) or chemisorbed species [41],[32]. The vacuum-grown sample has a higher contribution of V_O compared to the argon sample.

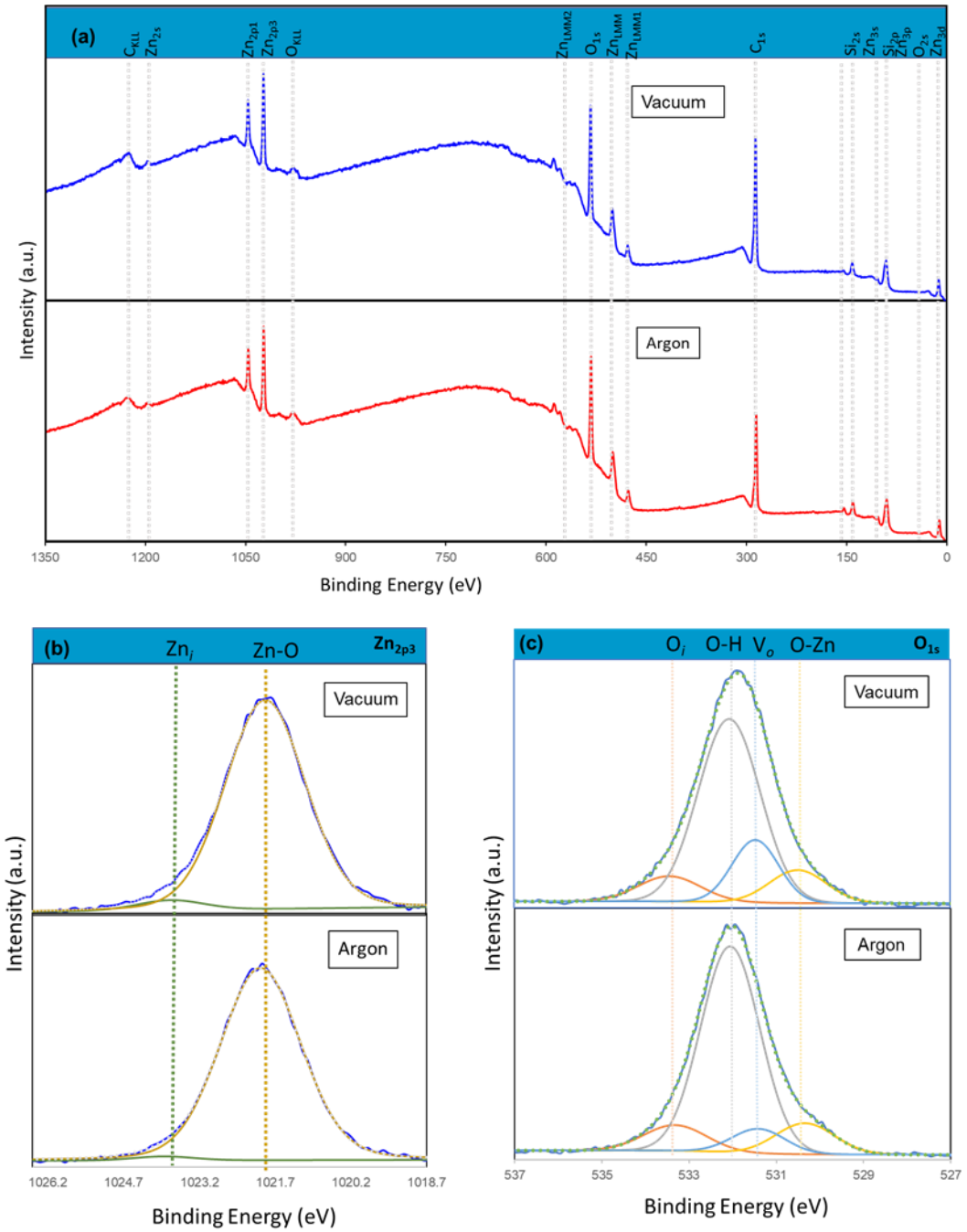

Fig. 4. Overview XPS spectra (a), and high-resolution XPS spectra for (b) Zn 2*p*3 core level and (c) O 1*s* core level.

3.3. Optical studies

Raman spectra excited by laser at 325 nm are illustrated in Fig. 5. The Resonance Raman scattering of ZnO nanomaterials is considerably less understood. This implies processes occurring in cases when the excitation wavelength approaches the energy band gap resonance of the nanomaterial. In the case of ZnO, the band gap is commonly located around 375 nm.

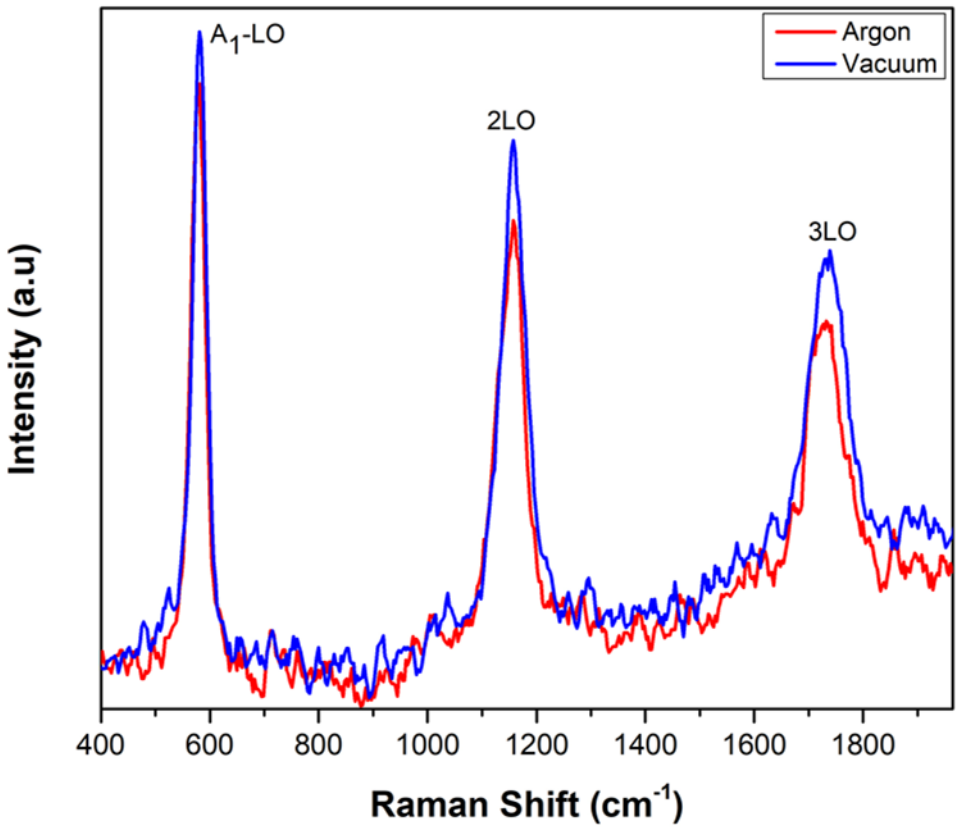

Fig. 5. Typical Raman spectra of the ZnO films (argon and vacuum) excited at 325 nm.

Fig 5. shows that for the Raman spectra, intense peaks attributed to the longitudinal optical (LO) band were recorded. A number of longitudinal optical (LO) multiphonon peaks are observed in

both resonant Raman spectra. Fig. 5 shows that the LO Raman modes for vacuum-grown ZnO films experience a slightly more intense resonance excitation compared to argon-grown films, due to the greater role of the Frölich interactions [48]. The frequency of the 1LO phonon peak located at 580 cm^{-1} corresponds to $E_1(LO)$, which can appear only when the c-axis of wurtzite ZnO is perpendicular to the sample surface [49],[50],[51].

The PL spectra measured at room temperature are presented in Fig. 6. For both ZnO samples, we observed two emission bands at room temperature, a strong and narrow UV emission band centered at 380 nm originated from the direct recombination of free exciton-related near-band-edge emission (NBE) in ZnO [52],[53]; and a weak and broad deep level emission (DLE) band in the visible range from 440 to 720 nm. The intensity of each spectrum was normalized to the intensity of the NBE emission for relative comparison. The FWHM of the NBE emission peaks are around 140 and 190 meV for the vacuum and argon samples, respectively. This broadening observed on the FWHM indicates that the quantity of intrinsic defects is higher for the argon sample [54].

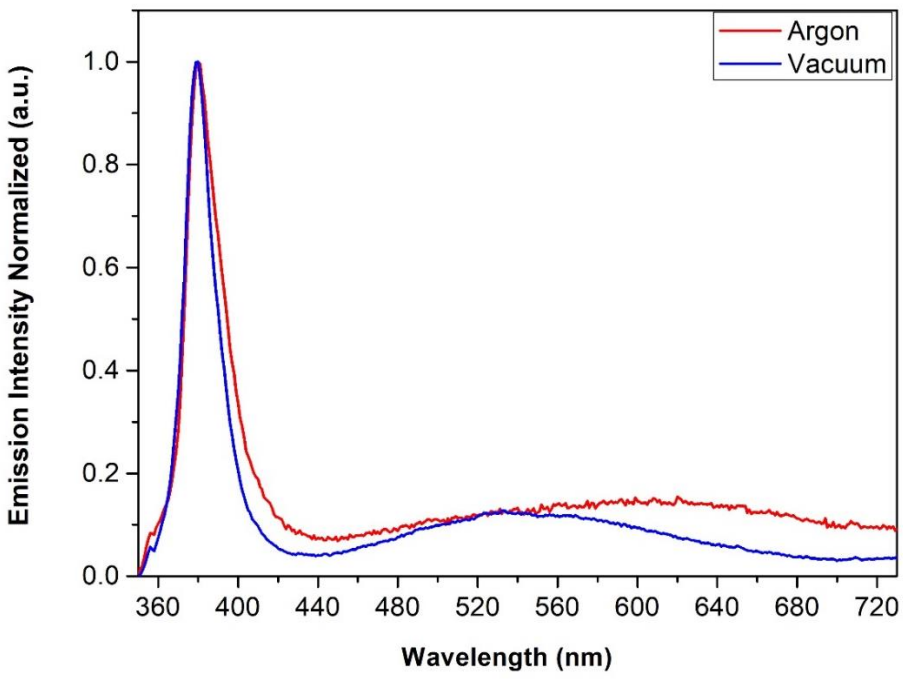

Fig. 6. PL spectra of ZnO films (argon/vacuum) at room temperature.

The broad emission band observed in the visible range is generally attributed to defects, and has the maximum emission intensity at around 520 nm "green luminescent band (GL)" and 590 nm "yellow luminescent band (YL)" for the vacuum and argon samples, respectively [55]. The origin of the DLE broadband is somewhat controversial, though there have been many reports on this emission. The commonly accepted explanation is that the GL is usually believed to be associated with V_O related to structural defects, trap-states or impurity-related radiative recombination processes; and the YL band could be associated to O_i. These PL results are in agreement with the previously presented XPS results.

3.4. Gas sensing results

The gas sensing properties of the PLD ZnO films towards NO_2 were studied at different operating temperatures i.e., 100, 150 and 200ºC. To test repeatability, five consecutive replicate measurements and recovery sequences were performed. Fig. 7 shows the typical behavior of an n-type semiconductor exposed to repeated response and recovery cycles of increasingly concentrated oxidizing (NO_2) species. Exposures to NO_2 (an electron acceptor) increase sensor resistance of the n-type material. Baseline recovery is performed under pure dry air. Furthermore, during the recovery cycle, when the target gas is removed and the sensors are only exposed to dry air, they return completely to their baseline resistance, which is shown in Fig 7. Baseline resistance is higher in vacuum-grown than in argon-grown ZnO films. This difference can be explained by the higher amount of oxygen vacancies present in vacuum-grown films, as revealed by XPS. The two types of sensors showed consistent and repeatable responses to various gas concentrations. The response of both films (vacuum, argon) is significantly stable because these sensors completely regain their initial baseline resistance after each cycle of measurement shown in Fig 7. The results show an increase in sensing response with each increment in analyte concentration. It has been found that recovery time was slightly longer for argon-grown films as compared to vacuum grown films. The recommended safe exposure limits to NO_2 is 1 ppm which is well above the lowest concentration tested in this paper [56].

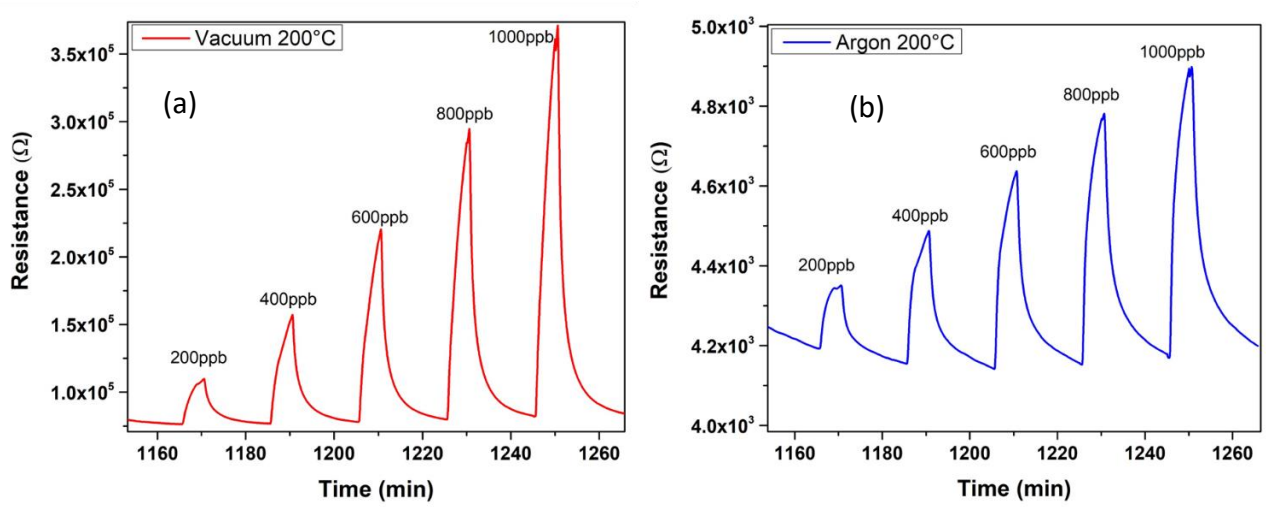

Fig. 7. Sensor resistance changes using the PLD ZnO films grown under vacuum (a) and argon (b) exposed to repeated exposure and recovery cycles to five increasing concentrations of NO_2. Sensors are operated at their optimal working temperatures (200ºC).

The (vacuum and argon) sensors were exposed to NO_2 at concentrations of 200, 400, 600, 800, and 1000 ppb at different working temperatures. The results are summarized in Fig. 8. When a vacuum sensor is operated at the lower temperatures tested of 100 and 150ºC, it shows moderate responsiveness. When the operating temperature is raised to 200ºC, a nearly 25-fold increase in NO_2 responsiveness is observed. The behavior of argon-grown films is very similar to the one displayed by vacuum films at 100ºC. When operated at 150 and 200ºC argon grown films show nearly a 10-fold enhancement in NO_2 responsiveness. Unlike vacuum-grown ZnO films, the responsiveness to nitrogen dioxide of argon-grown films is very similar when operated at 150 or 200ºC.

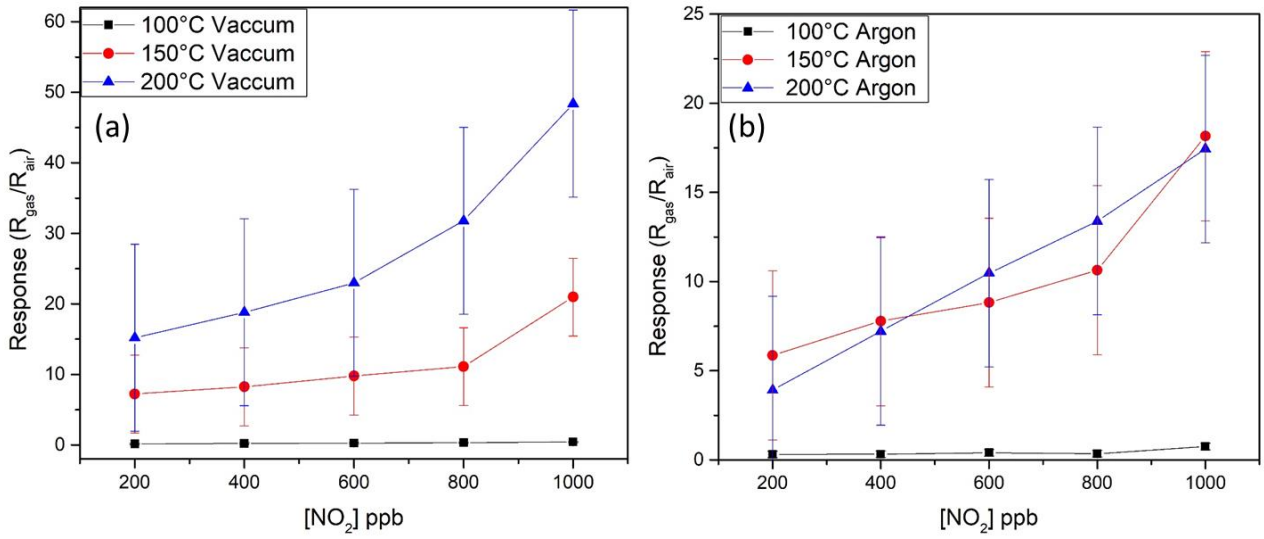

Fig. 8. (a) NO_2 sensing results obtained for vacuum-grown ZnO (b) and argon-grown ZnO at three different working temperatures.

The responsiveness for the two types of films towards NO_2 as a function of the operating temperature is summarized in Fig. 9. The responsiveness of vacuum or argon-grown films is very similar when operated at 100 or 150ºC. In contrast, vacuum-grown ZnO films clearly outperform argon-grown films when operated at 200ºC. Not only the response of vacuum-grown ZnO films is about 2.5 times higher than that of argon-grown films, but also the slope of the calibration curve is higher in vacuum-grown films, indicating that these show higher sensitivity to NO_2.

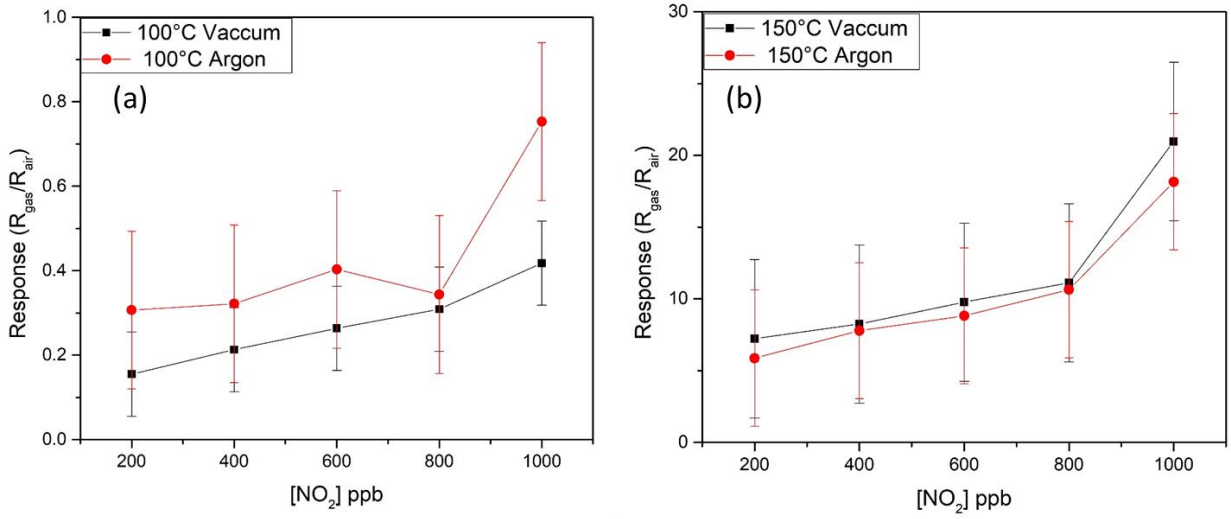

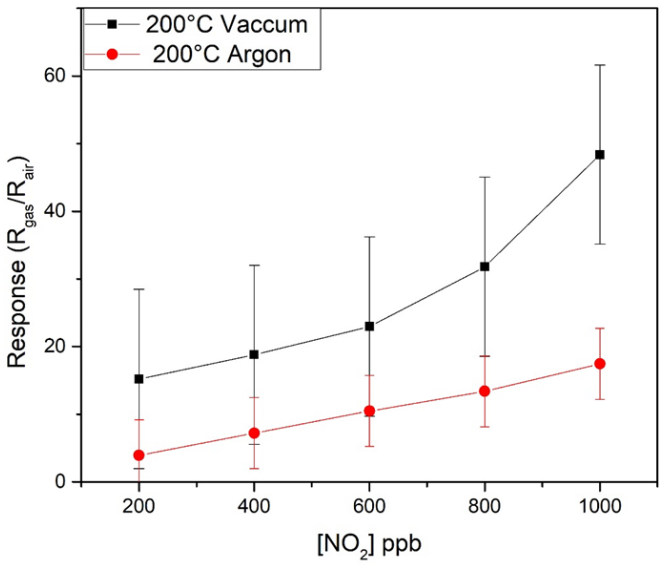

Fig. 9. Comparison of NO_2 sensor responsiveness for each of the 3 working temperatures tested.

3.5. PLD growth mechanism

In the PLD deposition process, the high-energy laser pulses interact with the target material, fixed in place by a substrate holder resulting in the evaporation of the surface layers. The evaporated material is vaporized from the target causing the formation of an expanding plasma. The plume of the ablated material gets deposited onto the substrate surface [32]. Plasma plumes consist of electrons, ions, atoms, or molecules. After ions reach the substrate, they settle on its surface in an atomic layer-by-layer growth process, called thin-film deposition. The different gas atmospheres and background pressures in the PLD process influence the film growth rate, stoichiometry, and crystallinity of the resulting film [57]. In this particular study, film growth in vacuum or in argon was implemented.

In the case of a vacuum-grown film, the plume angular distribution is formed by the collisions of the plume particles among themselves in the initial stage. The re-sputtering of ZnO from the film surface is also possible because there is no partial pressure of the gas inside the chamber. These effects favor the loss of oxygen and the growth of sub-stoichiometric oxides. The plume expansion behavior is even more complex often in the presence of environmental gas pressure [58].

In the presence of an argon atmosphere, the ablated species encounter a large number of collisions with argon gas molecules, which decreases the energy of the particles reaching at the substrate and decreases the size of the ablated plume. In addition, only ZnO clusters are deposited on the substrate and Zn^{2+} or Zn^{+} ions are not reaching the substrate. In such a case, secondary physical processes affect the plume expansion behavior, such as plume deceleration and splitting, shock-wave formation, thermalization, etc., as a consequence of plasma–background gas interaction [58].

As revealed by the different characterization techniques used, the differences in the background atmosphere during the PLD growth have an important impact of the morphology, microstructure and chemical composition of the ZnO films. Grown under vacuum or under argon, ZnO films exhibit a hexagonal wurtzite crystallite structure. However, while ZnO films grown under argon show a nearly single-crystalline structure with a c-axis orientation, vacuum-grown ZnO films are polycrystalline. Additionally, argon grown ZnO films are compact with a very homogeneous crystallite size (29 nm). In contrast, vacuum grown films are less compact (i.e., with high surface roughness), showing a wider range of crystallite sizes (with average size of 51 nm). The fact that film thickness differs by a factor of almost 2 between vacuum-grown and argon grown films and that re-sputtering is present under vacuum conditions only, may explain the differences in crystallinity observed. Finally, XPS and PL studies indicate that even though argon grown films are more defective (with dominant oxygen interstitials), vacuum grown ZnO films possess a higher number of oxygen vacancies. The less compact and sub-stoichiometric ZnO achieved via the PLD growth under vacuum conditions is more favorable for detecting NO_2.

3.6. Gas sensing mechanism

The gas-sensing mechanism in ZnO films is based mainly either by the adsorption of atmospheric oxygen onto the surface or by the direct reaction of lattice oxygen or interstitial oxygen with the test gases [59]. The type of adsorbed oxygen species depends on temperature as described in the four steps below [60].

At low temperatures (i.e., near room temperature), when ZnO is exposed to atmospheric oxygen, this oxygen is physically adsorbed to its surface in different molecular or atomic states without forming any ionic bond (see equation 1).

$$O_2(\text{gas}) \rightarrow O_2(\text{ads}) \quad \text{(Physical absorption)} \qquad (1)$$

As the temperature increases from 100 to 150ºC the dominant adsorbed oxygen species are molecular adsorbed oxygen, i.e., O_2^- (see equation 2).

$$e^- + O_2 \rightarrow O_2^- \qquad \text{(Ionic adsorption; } \leq 150°C) \qquad (2)$$

When the temperature is raised from 150 up to 300ºC the dominant adsorbed oxygen species become atomic O^- (see equation 3).

$$e^- + O_2^- \rightarrow 2O^- \quad \text{(Ionic adsorption; 150°C to 300°C)} \qquad (3)$$

A further increase in temperature above 300°C would lead to the formation of O^{2-}species (see equation 4).

$$e^- + O^- \rightarrow O^{2-} \qquad \text{(Ionic adsorption; } > 300°C) \qquad (4)$$

The evolution of oxygen adsorbed species with operating temperature involves the capture of electrons via the conduction band of the ZnO semiconductor and the formation of charged oxygen surface species (as described by equations 2 to 4). This results in the development of a depletion region at the surface of the grains of the gas sensitive material. Consequently, since different working temperatures of 100 ºC, 150 ºC and 200ºC have been used, different oxygen species would be found at such temperatures as well as co-exist in the transition temperatures. Besides the nature of adsorbed oxygen species having an impact on gas sensing properties, the type and the amount of defects in metal oxide films play also an important role [61]. Particularly, sub-stoichiometric metal oxides having a significant number of oxygen vacancies have been found to be more sensitive to gaseous species, as such vacancies generate an increased amount of adsorption sites

for oxidizing species (e.g., oxygen or even nitrogen dioxide). For ZnO, while the presence of surface defects is advantageous for detecting reducing species such as ethanol vapors, the presence of surface and deep-level defects is advantageous for detecting nitrogen dioxide. Hexagonal wurtzite ZnO has been found to be typically 50 times more responsive to NO_2 than to reducing species such as ethanol vapors [61].

For the NO_2 detection, the resistance of the ZnO sensor increases when exposed to such an oxidizing gas. The NO_2 molecules reach the metal oxide surface and are directly chemisorbed on the surface of ZnO films. These oxidizing molecules take more electrons from the conduction band of ZnO and thus, the width of the depletion region is further extended, which increases the resistance of ZnO films [59],[62],[63]. When the gas sensors are exposed to clean air again, adsorbed NO_2 is released and previously trapped electrons are injected into the conduction band, reducing the width of the depletion regions at grain boundaries. This translates into a decrease in sensor resistance (the original baseline resistance is regained).

According to the results presented in Fig. 8, clear differences arise between the intensity of response and sensitivity of argon and vacuum-grown films when these are operated at 200ºC. When operated at 200ºC, vacuum-grown films clearly outperform argon-grown films for detecting NO_2.

It has been found that gas sensitivity linearly increased with the PL intensity of V_O-related defects in both as-fabricated and defect-controlled ZnO nanowire gas sensors [64]. If we consider our PL analysis results, vacuum deposited films show the most intense visible emission band in their PL spectrum centered at 520 nm, which corresponds to the GL band. This means that the material with the higher number of V_O is the most sensitive to NO_2. This is further supported by the XPS analysis in which the amount of V_O is found to be higher in vacuum-grown films. This enhanced response could be due to the fact that at 200ºC, V_O are not completely healed with oxygen adsorbed species, leaving additional sites for adsorbing NO_2 molecules.

Besides V_O, other factors may influence gas sensitivity. In particular, the higher polycrystallinity (revealed by XRD) and higher surface texture (as revealed by SEM) found in vacuum-grown ZnO samples may also contribute to their higher response toward NO_2. Imperfections and defects can also play a role in the observed gas sensing properties by modifying the binding energies between adsorbed molecules and the semiconductor material. Such effects can be studied further using different in-situ, operando spectroscopic techniques (e.g. optical, vibrational, X-ray or scanning

probe) for gaining insights into the electronic structure and the surface chemistry associated with the adsorption of gas molecules [65] or by using noise spectrum methods, which have been found useful in providing information about adsorption/desorption energies, surface densities, the relative abundance of sites of different types and their relative occupancy by gaseous species [66]. Finally, hexagonal wurtzite ZnO films have been shown to be responsive to other oxidizing species such as ozone. However, ozone response in ZnO films has been reported at significantly higher operating temperatures (i.e., 300ºC) than the ones used here for detecting nitrogen dioxide [67].

4. Conclusions

To sum up, two different kinds of ZnO films were fabricated by PLD in different background atmospheres (i.e., vacuum or argon). The gas-sensing properties of NO_2 have been studied. By implementing room-temperature PL studies, it has been possible to establish that the PLD background atmosphere has an impact on the number of defects and the nature of these PL and XPS studies indicate that vacuum-grown ZnO films show a higher number of V_O than argon-grown films and this may explain the significantly higher response of the former in the detection of NO_2 at ppb levels, as oxygen vacancies can act as adsorption sites for the nitrogen dioxide molecule. The significant differences in the nature of defects in PLD ZnO films revealed by this study suggest that the use of different backgrounds during the growth process can be used as a suitable methodology for the engineering of defects in PLD-grown nanomaterials, thus achieving functional materials with controlled properties. This approach is not only suitable for tailoring gas sensing properties but could also be in photovoltaics, electronic devices, or light-emitting diodes. The role of imperfections and surface defects in the gas sensing properties of ZnO films will be further studied in the near future by in-operando spectroscopic techniques.

Declaration of Competing Interest

The authors declare that they have no known competing financial interests or personal relationships that could have appeared to influence the work reported in this paper.

Acknowledgments

This work has been partially supported by the Croatian Science Foundation under the projects IP-2014-09-7046 and IP-2019-04-6418 and by the project co-financed by the Croatian Government and the European Union through the European Regional Development Fund - the Competitiveness and Cohesion Operational Programme (KK.01.1.1.01.0001). E. L. is supported by the Catalan Institution for Research and Advanced Studies via the 2018 Edition of the ICREA Academia Award.

References

[1] I. Manisalidis, E. Stavropoulou, A. Stavropoulos, and E. Bezirtzoglou, 'Environmental and Health Impacts of Air Pollution: A Review', *Front. Public Health*, vol. 8, p. 14, Feb. 2020, doi: 10.3389/fpubh.2020.00014.

[2] S. Khomenko *et al.*, 'Premature mortality due to air pollution in European cities: a health impact assessment', *Lancet Planet. Health*, vol. 5, no. 3, pp. e121–e134, Mar. 2021, doi: 10.1016/S2542-5196(20)30272-2.

[3] T. Bourdrel, M.-A. Bind, Y. Béjot, O. Morel, and J.-F. Argacha, 'Cardiovascular effects of air pollution', *Arch. Cardiovasc. Dis.*, vol. 110, no. 11, pp. 634–642, Nov. 2017, doi: 10.1016/j.acvd.2017.05.003.

[4] W. J. Gauderman *et al.*, 'Association of Improved Air Quality with Lung Development in Children', *N. Engl. J. Med.*, vol. 372, no. 10, pp. 905–913, Mar. 2015, doi: 10.1056/NEJMoa1414123.

[5] D. Gielen, F. Boshell, D. Saygin, M. D. Bazilian, N. Wagner, and R. Gorini, 'The role of renewable energy in the global energy transformation', *Energy Strategy Rev.*, vol. 24, pp. 38–50, Apr. 2019, doi: 10.1016/j.esr.2019.01.006.

[6] D. Sofia, F. Gioiella, N. Lotrecchiano, and A. Giuliano, 'Mitigation strategies for reducing air pollution', *Environ. Sci. Pollut. Res.*, vol. 27, no. 16, pp. 19226–19235, Jun. 2020, doi: 10.1007/s11356-020-08647-x.

[7] E. González, J. Casanova-Chafer, A. Romero, X. Vilanova, J. Mitrovics, and E. Llobet, 'LoRa Sensor Network Development for Air Quality Monitoring or Detecting Gas Leakage Events', *Sensors*, vol. 20, no. 21, Art. no. 21, Jan. 2020, doi: 10.3390/s20216225.
[8] A. T. John, K. Murugappan, D. R. Nisbet, and A. Tricoli, 'An Outlook of Recent Advances in Chemiresistive Sensor-Based Electronic Nose Systems for Food Quality and Environmental Monitoring', *Sensors*, vol. 21, no. 7, p. 2271, Mar. 2021, doi: 10.3390/s21072271.
[9] M. A. H. Khan, M. V. Rao, and Q. Li, 'Recent Advances in Electrochemical Sensors for Detecting Toxic Gases: NO2, SO2 and H2S', *Sensors*, vol. 19, no. 4, p. 905, Feb. 2019, doi: 10.3390/s19040905.
[10] R. Kumar, O. Al-Dossary, G. Kumar, and A. Umar, 'Zinc Oxide Nanostructures for NO2 Gas-Sensor Applications: A Review', *Nano-Micro Lett.*, vol. 7, no. 2, pp. 97–120, 2015, doi: 10.1007/s40820-014-0023-3.
[11] G. Neri, 'First Fifty Years of Chemoresistive Gas Sensors', *Chemosensors*, vol. 3, no. 1, Art. no. 1, Mar. 2015, doi: 10.3390/chemosensors3010001.
[12] J. P. Cheng, J. Wang, Q. Q. Li, H. G. Liu, and Y. Li, 'A review of recent developments in tin dioxide composites for gas sensing application', *J. Ind. Eng. Chem.*, vol. 44, pp. 1–22, Dec. 2016, doi: 10.1016/j.jiec.2016.08.008.
[13] D. Degler, U. Weimar, and N. Barsan, 'Current Understanding of the Fundamental Mechanisms of Doped and Loaded Semiconducting Metal-Oxide-Based Gas Sensing Materials', *ACS Sens.*, vol. 4, no. 9, pp. 2228–2249, Sep. 2019, doi: 10.1021/acssensors.9b00975.
[14] L. Zhu and W. Zeng, 'Room-temperature gas sensing of ZnO-based gas sensor: A review', *Sens. Actuators Phys.*, vol. 267, pp. 242–261, Nov. 2017, doi: 10.1016/j.sna.2017.10.021.
[15] N. A. Abdullah, Z. Khusaimi, and M. Rusop, 'A Review on Zinc Oxide Nanostructures: Doping and Gas Sensing', *Adv. Mater. Res.*, vol. 667, pp. 329–332, 2013, doi: 10.4028/www.scientific.net/AMR.667.329.
[16] Z. Fan and J. G. Lu, 'Zinc Oxide Nanostructures: Synthesis and Properties', *J. Nanosci. Nanotechnol.*, vol. 5, no. 10, pp. 1561–1573, Oct. 2005, doi: 10.1166/jnn.2005.182.
[17] D. Nunes *et al.*, 'Metal oxide nanostructures for sensor applications', *Semicond. Sci. Technol.*, vol. 34, no. 4, p. 043001, Mar. 2019, doi: 10.1088/1361-6641/ab011e.
[18] Q. Peng, Y. Qin, Q. Peng, and Y. Qin, *ZnO Nanowires and Their Application for Solar Cells*. IntechOpen, 2011. doi: 10.5772/17923.
[19] V. Consonni, J. Briscoe, E. Kärber, X. Li, and T. Cossuet, 'ZnO nanowires for solar cells: a comprehensive review', *Nanotechnology*, vol. 30, no. 36, p. 362001, Jun. 2019, doi: 10.1088/1361-6528/ab1f2e.
[20] D. Vanmaekelbergh and L. K. van Vugt, 'ZnO nanowire lasers', *Nanoscale*, vol. 3, no. 7, pp. 2783–2800, Jul. 2011, doi: 10.1039/C1NR00013F.
[21] T. Hirao *et al.*, 'Bottom-Gate Zinc Oxide Thin-Film Transistors (ZnO TFTs) for AM-LCDs', *IEEE Trans. Electron Devices*, vol. 55, no. 11, pp. 3136–3142, Nov. 2008, doi: 10.1109/TED.2008.2003330.
[22] F. Rahman, 'Zinc oxide light-emitting diodes: a review', *Opt. Eng.*, vol. 58, no. 1, p. 010901, Jan. 2019, doi: 10.1117/1.OE.58.1.010901.
[23] Ü. Özgür, D. Hofstetter, and H. Morkoç, 'ZnO Devices and Applications: A Review of Current Status and Future Prospects', *Proc. IEEE*, vol. 98, no. 7, pp. 1255–1268, Jul. 2010, doi: 10.1109/JPROC.2010.2044550.
[24] Y. W. Heo *et al.*, 'ZnO nanowire growth and devices', *Mater. Sci. Eng. R Rep.*, vol. 47, no. 1, pp. 1–47, Dec. 2004, doi: 10.1016/j.mser.2004.09.001.
[25] B. Liu and H. C. Zeng, 'Hydrothermal Synthesis of ZnO Nanorods in the Diameter Regime of 50 nm', *J. Am. Chem. Soc.*, vol. 125, no. 15, pp. 4430–4431, Apr. 2003, doi: 10.1021/ja0299452.

[26] J. Guo, J. Zhang, M. Zhu, D. Ju, H. Xu, and B. Cao, 'High-performance gas sensor based on ZnO nanowires functionalized by Au nanoparticles', *Sens. Actuators B Chem.*, vol. 199, pp. 339–345, Aug. 2014, doi: 10.1016/j.snb.2014.04.010.
[27] S. Agarwal *et al.*, 'Gas sensing properties of ZnO nanostructures (flowers/rods) synthesized by hydrothermal method', *Sens. Actuators B Chem.*, vol. 292, pp. 24–31, Aug. 2019, doi: 10.1016/j.snb.2019.04.083.
[28] P. F. Carcia, R. S. McLean, M. H. Reilly, and G. Nunes, 'Transparent ZnO thin-film transistor fabricated by rf magnetron sputtering', *Appl. Phys. Lett.*, vol. 82, no. 7, pp. 1117–1119, Feb. 2003, doi: 10.1063/1.1553997.
[29] O. A. Fouad, A. A. Ismail, Z. I. Zaki, and R. M. Mohamed, 'Zinc oxide thin films prepared by thermal evaporation deposition and its photocatalytic activity', *Appl. Catal. B Environ.*, vol. 62, no. 1, pp. 144–149, Jan. 2006, doi: 10.1016/j.apcatb.2005.07.006.
[30] S. I. Boyadjiev, V. Georgieva, R. Yordanov, Z. Raicheva, and I. M. Szilágyi, 'Preparation and characterization of ALD deposited ZnO thin films studied for gas sensors', *Appl. Surf. Sci.*, vol. 387, pp. 1230–1235, Nov. 2016, doi: 10.1016/j.apsusc.2016.06.007.
[31] A. I. Khudiar and A. M. Ofui, 'Effect of pulsed laser deposition on the physical properties of ZnO nanocrystalline gas sensors', *Opt. Mater.*, vol. 115, p. 111010, May 2021, doi: 10.1016/j.optmat.2021.111010.
[32] R. Kumar, G. Kumar, and A. Umar, 'Pulse laser deposited nanostructured ZnO thin films: a review', *J. Nanosci. Nanotechnol.*, vol. 14, no. 2, pp. 1911–1930, Feb. 2014, doi: 10.1166/jnn.2014.9120.
[33] G. Atanasova *et al.*, 'Metal-oxide nanostructures produced by PLD in open air for gas sensor applications', *Appl. Surf. Sci.*, vol. 470, pp. 861–869, Mar. 2019, doi: 10.1016/j.apsusc.2018.11.178.
[34] F. L. Kuo, M.-T. Lin, B. A. Mensah, T. W. Scharf, and N. D. Shepherd, 'A comparative study of the photoluminescence and conduction mechanisms of low temperature pulsed laser deposited and atomic layer deposited zinc oxide thin films', *Phys. Status Solidi A*, vol. 207, no. 11, pp. 2487–2491, 2010, doi: 10.1002/pssa.201026152.
[35] O. A. Ageev *et al.*, 'Nanocrystalline ZnO Films Grown by PLD for NO2 and NH3 Sensor', *Appl. Mech. Mater.*, vol. 475–476, pp. 446–450, 2014, doi: 10.4028/www.scientific.net/AMM.475-476.446.
[36] Z. G. Zhang *et al.*, 'Effects of oxygen pressures on pulsed laser deposition of ZnO films', *Phys. E Low-Dimens. Syst. Nanostructures*, vol. 39, no. 2, pp. 253–257, Sep. 2007, doi: 10.1016/j.physe.2007.05.028.
[37] R. Kek *et al.*, 'Effects of pressure and substrate temperature on the growth of Al-doped ZnO films by pulsed laser deposition', *Mater. Res. Express*, vol. 7, no. 1, p. 016414, Jan. 2020, doi: 10.1088/2053-1591/ab62f8.
[38] D. Fasquelle, S. Députier, V. Bouquet, and M. Guilloux-Viry, 'Effect of the Microstructure of ZnO Thin Films Prepared by PLD on Their Performance as Toxic Gas Sensors', *undefined*, 2022, Accessed: Aug. 31, 2022. [Online]. Available: https://www.semanticscholar.org/paper/Effect-of-the-Microstructure-of-ZnO-Thin-Films-by-Fasquelle-D%C3%A9putier/d6cf838fe3786481bca5f526bd5c59b9db14a25e
[39] J. Chu, X. Peng, Z. Wang, and P. Feng, 'Sensing performances of ZnO nanostructures grown under different oxygen pressures to hydrogen', *Mater. Res. Bull.*, vol. 47, no. 12, pp. 4420–4426, Dec. 2012, doi: 10.1016/j.materresbull.2012.09.037.
[40] X. M. Fan, J. S. Lian, Z. X. Guo, and H. J. Lu, 'Microstructure and photoluminescence properties of ZnO thin films grown by PLD on Si(111) substrates', *Appl. Surf. Sci.*, vol. 239, no. 2, pp. 176–181, Jan. 2005, doi: 10.1016/j.apsusc.2004.05.144.
[41] V. Kumar *et al.*, 'The role of growth atmosphere on the structural and optical quality of defect free ZnO films for strong ultraviolet emission', *Laser Phys.*, vol. 24, p. 105704, Oct. 2014, doi: 10.1088/1054-660X/24/10/105704.

[42] B. ElZein, Y. Yao, A. S. Barham, E. Dogheche, and G. E. Jabbour, 'Toward the Growth of Self-Catalyzed ZnO Nanowires Perpendicular to the Surface of Silicon and Glass Substrates, by Pulsed Laser Deposition', *Materials*, vol. 13, no. 19, p. 4427, Oct. 2020, doi: 10.3390/ma13194427.
[43] Z. Wang *et al.*, 'Vacancy cluster in ZnO films grown by pulsed laser deposition', *Sci. Rep.*, vol. 9, no. 1, Art. no. 1, Mar. 2019, doi: 10.1038/s41598-019-40029-3.
[44] D. Padilla-Rueda, J. M. Vadillo, and J. J. Laserna, 'Room temperature pulsed laser deposited ZnO thin films as photoluminiscence gas sensors', *Appl. Surf. Sci.*, vol. 259, pp. 806–810, Oct. 2012, doi: 10.1016/j.apsusc.2012.07.128.
[45] Y. Wang, X. Chen, L. Wang, S. Yang, and Z. Feng, 'Properties of ZnO thin film on Al2O3 substrate prepared by pulsed laser deposition under different substrate temperature', *Phys. Procedia*, vol. 18, pp. 85–90, Jan. 2011, doi: 10.1016/j.phpro.2011.06.063.
[46] N. Fujimura, T. Nishihara, S. Goto, J. Xu, and T. Ito, 'Control of preferred orientation for ZnOx films: control of self-texture', *J. Cryst. Growth*, vol. 130, no. 1, pp. 269–279, May 1993, doi: 10.1016/0022-0248(93)90861-P.
[47] A. V. Shchukarev and D. V. Korolkov, 'XPS Study of group IA carbonates', *Cent. Eur. J. Chem.*, vol. 2, no. 2, pp. 347–362, Jun. 2004, doi: 10.2478/BF02475578.
[48] X. Zhu, H. Wu, Z. Yuan, J. Kong, and W. Shen, 'Multiphonon resonant Raman scattering in N-doped ZnO', *J. Raman Spectrosc.*, vol. 40, no. 12, pp. 2155–2161, 2009, doi: 10.1002/jrs.2385.
[49] R. Zhang, P.-G. Yin, N. Wang, and L. Guo, 'Photoluminescence and Raman scattering of ZnO nanorods', *Solid State Sci.*, vol. 11, no. 4, pp. 865–869, Apr. 2009, doi: 10.1016/j.solidstatesciences.2008.10.016.
[50] N. Ashkenov *et al.*, 'Infrared dielectric functions and phonon modes of high-quality ZnO films', *J. Appl. Phys.*, vol. 93, no. 1, pp. 126–133, Jan. 2003, doi: 10.1063/1.1526935.
[51] K. A. Alim, V. A. Fonoberov, M. Shamsa, and A. A. Balandin, 'Micro-Raman investigation of optical phonons in ZnO nanocrystals', *J. Appl. Phys.*, vol. 97, no. 12, p. 124313, Jun. 2005, doi: 10.1063/1.1944222.
[52] M. R. Wagner, 'Fundamental properties of excitons and phonons in ZnO: A spectroscopic study of the dynamics, polarity, and effects of external fields', 2010. doi: 10.14279/DEPOSITONCE-2666.
[53] W. Shan *et al.*, 'Nature of room-temperature photoluminescence in ZnO', *Appl. Phys. Lett.*, vol. 86, no. 19, p. 191911, May 2005, doi: 10.1063/1.1923757.
[54] F. Güell *et al.*, 'Raman and photoluminescence properties of ZnO nanowires grown by a catalyst-free vapor-transport process using ZnO nanoparticle seeds', *Phys. Status Solidi B*, vol. 253, no. 5, pp. 883–888, 2016, doi: 10.1002/pssb.201552651.
[55] F. Güell and P. R. Martínez-Alanis, 'Tailoring the Green, Yellow and Red defect emission bands in ZnO nanowires via the growth parameters', *J. Lumin.*, vol. 210, pp. 128–134, Jun. 2019, doi: 10.1016/j.jlumin.2019.02.017.
[56] J. S. Ji *et al.*, 'NO2 and PM2.5 air pollution co-exposure and temperature effect modification on pre-mature mortality in advanced age: a longitudinal cohort study in China', *Environ. Health*, vol. 21, no. 1, p. 97, Oct. 2022, doi: 10.1186/s12940-022-00901-8.
[57] I. N. Mihailescu and A. P. Caricato, Eds., *Pulsed Laser Ablation: Advances and Applications in Nanoparticles and Nanostructuring Thin Films*, 1st edition. Singapore: Jenny Stanford Publishing, 2018.
[58] S. S. Harilal, C. V. Bindhu, M. S. Tillack, F. Najmabadi, and A. C. Gaeris, 'Internal structure and expansion dynamics of laser ablation plumes into ambient gases', *J. Appl. Phys.*, vol. 93, no. 5, pp. 2380–2388, Mar. 2003, doi: 10.1063/1.1544070.
[59] M. J. S. Spencer and I. Yarovsky, 'ZnO Nanostructures for Gas Sensing: Interaction of NO2, NO, O, and N with the ZnO(10$\bar{1}$0) Surface', *J. Phys. Chem. C*, vol. 114, no. 24, pp. 10881–10893, Jun. 2010, doi: 10.1021/jp1016938.

[60] M. Jiao *et al.*, 'Comparison of NO2 Gas-Sensing Properties of Three Different ZnO Nanostructures Synthesized by On-Chip Low-Temperature Hydrothermal Growth', *J. Electron. Mater.*, vol. 47, no. 1, pp. 785–793, Jan. 2018, doi: 10.1007/s11664-017-5829-6.
[61] S. Roso, F. Güel, P. R. Martínez-Alanis, A. Urakawa, and E. Llobet, 'Synthesis of ZnO nanowires and impacts of their orientation and defects on their gas sensing properties', 2016, doi: 10.1016/j.snb.2016.02.048.
[62] A. Tamvakos, K. Korir, D. Tamvakos, D. Calestani, G. Cicero, and D. Pullini, 'NO2 Gas Sensing Mechanism of ZnO Thin-Film Transducers: Physical Experiment and Theoretical Correlation Study', *ACS Sens.*, vol. 1, no. 4, pp. 406–412, Apr. 2016, doi: 10.1021/acssensors.6b00051.
[63] C.-J. Chang, C.-Y. Lin, J.-K. Chen, and M.-H. Hsu, 'Ce-doped ZnO nanorods based low operation temperature NO2 gas sensors', *Ceram. Int.*, vol. 7 Part B, no. 40, pp. 10867–10875, 2014, doi: 10.1016/j.ceramint.2014.03.080.
[64] M. W. Ahn *et al.*, 'Gas sensing properties of defect-controlled ZnO-nanowire gas sensor', *Appl. Phys. Lett.*, vol. 93, no. 26, 2008, doi: 10.1063/1.3046726.
[65] A. Sharma and C. S. Rout, 'Advances in understanding the gas sensing mechanisms by in situ and operando spectroscopy', *J. Mater. Chem. A*, vol. 9, no. 34, pp. 18175–18207, Aug. 2021, doi: 10.1039/D1TA05054K.
[66] S. Andrić, I. Jokić, J. Stevanović, M. Spasenović, and M. Frantlović, 'Noise Spectrum as a Source of Information in Gas Sensors Based on Liquid-Phase Exfoliated Graphene', *Chemosensors*, vol. 10, no. 6, Art. no. 6, Jun. 2022, doi: 10.3390/chemosensors10060224.
[67] W. A. dos Santos Silva, B. S. de Lima, M. I. B. Bernardi, and V. R. Mastelaro, 'Enhancement of the ozone-sensing properties of ZnO through chemical-etched surface texturing', *J. Nanoparticle Res.*, vol. 24, p. 96, May 2022, doi: 10.1007/s11051-022-05479-3.

- Kamran Ali Syed received an MSc degree in Physics from Universität Siegen (Germany), and is currently pursuing a Ph.D. degree in Physics at Institute Ruđer Bošković Croatia). His research is focused on the development of gas-sensing materials, Gas sensors, Nanotechnology.

- Nikša Krstulović, has MSc and Ph.D. in Physics. He works as a Senior research associate at the Institute of Physics, Croatia. He is an expert in laser plasmas, cold plasmas, plasma diagnostics, PLD and nanotechnology. He is a Plasma and Laser Applied Research Group leader at Centre for Advanced Laser Techniques.

- Juan Casanova-Cháfer, has MSc and Ph.D. in Chemistry. He works as a post-doctoral fellow at Universitat Rovira i Virgili in Tarragona (Spain). He is an expert in Gas Sensors, Carbon Nanomaterials, Thin Films, and Nanotechnology.

- Eduard Llobet, is a full professor at the Department of Electronic Engineering of the Universitat Rovira i Virgili in Tarragona (Spain). He was awarded a Ph.D. in 1997 from the Technical University of Catalonia (Barcelona). He is an expert in Gas sensors, low-dimensional metal oxides, MEMS or flexible platforms.

- Frank Güell, has MSc and Ph.D. in Physics. He works as an associate professor at Universitat de Barcelona, Catalunya. He is an expert in nanomaterials, photoluminescence and optical spectroscopy.

- Paulina R. Martínez-Alanis, has MSc and Ph.D. in Chemisrty. She works as an assistant professor at Universitat de Barcelona, Catalunya. She is an expert in nanomaterials and X-ray photoelectron spectroscopy.

- Marijan Marciuš, has MSc and Ph.D. in Physics. He works as a Senior research associate at the Institute of Physics, Croatia. He is an expert in PLD, nanotechnology, and laser ablation synthesis.

- Ekaterina Shagieva, has Ph.D. in Microbiology. She works as a post-doctoral fellow at the Institute of Physics of the Czech Academy of Sciences. She is a specialist in Raman, photoluminescence, FTIR (Fourier transform infrared spectroscopy), and molecular biological methods.

- Hrvoje Gebavi, has MSc in physics and a Ph.D. in material science. He works as a Research Associate at Institut Ruđer Bošković, Division of Materials Physics, Laboratory for Molecular Physics and Synthesis of New Materials. He is an expert in sensors, nanotechnology, and Raman spectroscopy.

- Davor Ristic´, has MSc and Ph.D. in physics. He works as a Research Associate at Institut Ruđer Bošković, Division of Materials Physics, Laboratory for Molecular Physics and

Synthesis of New Materials. He is an expert in sensors, nanotechnology, and micro-sphere resonators.

- Nikola Baran, has MSc and Ph.D. in Physics. He works as a Post-doc at Institut Ruđer Bošković, Division of Materials Physics, He is an expert in gas sensors, electrochemical etching and porous silicon.

- Mile Ivanda, has MSc and Ph.D. in physics. He works as a full professor and head of the Laboratory for Molecular Physics and Synthesis of New Materials at Institut Ruđer Bošković. He is an expert in sensors, nanotechnology, and Raman spectroscopy.